Original Research

Diffusion Kurtosis Imaging Study of Prostate Cancer: Preliminary Findings

Chiharu Tamura, MD,[1] Hiroshi Shinmoto, MD, PhD,[1]* Shigeyoshi Soga, MD, PhD,[1] Teppei Okamura, MD,[1] Hiroki Sato, MS,[2] Tomoyuki Okuaki, MS, RT,[3] Yuxi Pang, PhD,[4] Shigeru Kosuda, MD, PhD,[1] and Tatsumi Kaji, MD, PhD[1]

Purpose: To evaluate the differences in parameters of diffusion kurtosis imaging (DKI) between prostate cancer, benign prostatic hyperplasia (BPH), and benign peripheral zone (PZ).

Materials and Methods: Twenty-four foci of prostate cancer, 41 BPH nodules (14 stromal and 27 nonstromal hyperplasia), and 20 benign PZ from 20 patients who underwent radical prostatectomy were investigated. Diffusion-weighted imaging (DWI) was performed using 11 b-values (0–1500 s/mm^2). DKI model relates DWI signal decay to parameters that reflect non-Gaussian diffusion coefficient (*D*) and deviations from normal distribution (*K*). A mixed model analysis of variance and receiver operating characteristic (ROC) analyses were performed to assess the statistical significance of the metrics of DKI and apparent diffusion coefficient (ADC).

Results: *K* was significantly higher in prostate cancer and stromal BPH than in benign PZ (1.19 ± 0.24 and 0.99 ± 0.28 versus 0.63 ± 0.23, $P < 0.001$ and $P < 0.001$, respectively). *K* showed a trend toward higher levels in prostate cancer than in stromal BPH (1.19 ± 0.24 versus 0.99 ± 0.28, $P = 0.051$). On the ROC analyses, a significant difference in area under the curve was not observed between *K* and ADC, however, *K* showed the highest sensitivity among three parameters.

Conclusion: DKI may contribute to the imaging diagnosis of prostate cancer, especially in the differential diagnosis of prostate cancer and BPH.

Key Words: magnetic resonance imaging; diffusion; kurtosis; prostate cancer; benign prostatic hyperplasia
J. Magn. Reson. Imaging 2014;40:723–729.

PROSTATE CANCER IS the second most common cancer among men (1), and its incidence rates remain high in many countries worldwide, including in western and northern Europe and Oceania (2). Although the prostate cancer mortality rate has declined by 39% from 1991 to 2008 in the United States, prostate cancer is still the most commonly diagnosed nonskin cancer and the second leading cause of cancer death among men in 2012 (3). The baseline evaluation of newly diagnosed patients is primarily carried out through serum prostate-specific antigen (PSA) tests, digital rectal examinations, trans-rectal ultrasounds (TRUS), and the histological results of prostatic biopsies (4). However, the detection rate and the prediction of the local extent of the disease remain unsatisfactory with these methods (5–7).

MRI of prostate cancer provides excellent anatomic information and has been considered sensitive for the detection of prostate cancer. Prostate cancer typically manifests as hypointense foci on T2-weighted images (T2WI), enhancing more and washing out faster than benign tissues with dynamic contrast-enhanced study (8,9). However, various conditions such as prostate intra-epithelial neoplasm, prostatitis, hemorrhage, atrophy, scars, and post-treatment changes can mimic cancer in the peripheral zone (PZ) on T2WI (10,11). In addition, benign prostatic hyperplasia (BPH) can be similar to prostate cancer in the transitional zone (TZ) in terms of T2-signal intensities and dynamic kinetics of gadolinium (12). A capsule-like structure, common occurrence in BPH nodules, is also observed in some cases of prostate cancer (12). Thus, the specificity for prostate cancer on T2WI is generally considered insufficient.

Diffusion-weighted imaging (DWI) and its metric, the apparent diffusion coefficient (ADC), appears to improve diagnostic performance and can be a useful adjunct to conventional anatomic imaging for identifying tumor foci in prostate cancer (13–17). ADC values of prostate cancer are generally lower than those of normal prostate tissues, particularly in the PZ. The standard DWI is based on free diffusion and a conventional monoexponential model. However, in biologic tissues, diffusion is restricted by the presence of various barriers, such as cellular compartments and

[1]Department of Radiology, National Defense Medical College, Saitama, Japan.
[2]Department of Preventive Medicine and Public Health, National Defense Medical College, Saitama, Japan.
[3]Philips Electronics Japan, Tokyo, Japan.
[4]Philips Healthcare, Cleveland, USA.
*Address reprint requests to: H. Shinmoto, 3-2, Namiki, Tokorozawa, Saitama, 359-8513, Japan. E-mail: shinmoto@ga2.so-net.ne.jp
Received June 19, 2013; Accepted August 9, 2013.
DOI 10.1002/jmri.24379
View this article online at wileyonlinelibrary.com.

membranes. A new diffusion metric, diffusion kurtosis imaging (DKI), is a non-Gaussian DWI method that was first described by Jensen et al in 2005 (18). This imaging analysis method is considered to be able to more accurately reflect the microstructural complexity of tissue structures than the conventional monoexponential model (18–20). DKI provides an estimate for the excess kurtosis of the diffusion displacement probability distribution (18). The parameter *K* can reflect deviations from normal distribution in restricted water diffusion. In view of the complex histologic composition of prostate cancer, DKI could potentially serve as a more effective model for the assessment of prostate cancer than standard DWI. Thus, the purpose of this study was to evaluate the differences in parameters of DKI and ADC between prostate cancer, BPH, and benign PZ.

MATERIALS AND METHODS

Patients

Our institutional review board approved this retrospective study and deemed that patient informed consent was not required. In this study, the standard of reference was histology following radical prostatectomy. Between July 2011 and July 2012, 156 consecutive patients with elevated PSA levels underwent MRI. The inclusion criteria for the patients of this study were (i) positive results for prostate cancer by radical prostatectomy, (ii) an obvious region of cancer on MRI, with histologically positive results for cancer in the corresponding region, and (iii) a normal-appearing contralateral PZ on MRI, with no cancerous tissue revealed by histopathology in the corresponding PZ area. From a series of 156 patients, 65 patients had positive results for prostate cancer with subsequent TRUS-guided biopsies. Of these 65 patients, 20 patients met our inclusion criteria. A summary of characteristics for the 20 patients is analyzed in Table 1.

Table 1
Characteristics of 20 Patients With Prostate Cancer*

Characteristic	Data
Age (years)	
Mean	66.4 ± 6.1
Range	52 – 75
Prostate-specific antigen level (ng/ml)	
Mean	8.48 ± 5.2
Range	3.49 – 21.52
Pathologic stage	
T2a	4
T2b	1
T2c	15
Gleason grade	
3 + 3	3
3 + 4	6
4 + 3	9
4 + 5	1
5 + 4	1
Interval between MRI and radical prostatectomy (days)	
Mean	78 ± 51
Range	5 – 184

*Unless otherwise indicated, data are number of patients.

MRI

All examinations were performed using a 3 Tesla (T) MRI scanner (Achieva, Philips Healthcare, Eindhoven, the Netherlands) using a 16-channel phased-array coil. For preventing artifacts from bowel peristalsis, 1 mg of intramuscular glucagon (Glucagon G Novo, Eisai, Tokyo, Japan) was administered immediately before the MRI examination.

The examinations included axial and coronal T2WI (repetition time/echo time [TR/TE] = 4000–4600 ms/70–80 ms; echo train length = 10; matrix sizes = 512 × 256; zero-filled interporation [ZIP] = 1024; section thickness/interslice gap = 3.5 mm/0.1 mm; field of view [FOV] = 160–180 × 160–180 mm; acquisition time = 7 min 29 s), axial DWI (TR/TE = 5000 ms/49 ms; matrix sizes = 80 × 80; ZIP = 1024; section thickness/interslice gap = 3.5 mm/0.1 mm; FOV = 240 × 240 mm; two excitations; acquisition time = 7 min 15 s), and gadolinium-enhanced dynamic MRI (enhanced T1-weighted high-resolution isotropic volume excitation; TR/TE = 3.8 ms/1.9 ms; flip angle = 15°; slice thickness = 3.0 mm (ZIP = 1.5 mm); scan matrix = 240 × 194 (ZIP = 512); FOV = 240 × 240 mm; acquisition time = 25 s). DWI was performed before dynamic MRI with the diffusion sensitization gradients oriented along three orthogonal directions at 11 b-values (0, 10, 20, 30, 50, 80, 100, 200, 400, 1000, and 1500 s/mm^2) with a parallel imaging technique, sensitivity encoding reduction factor of two. In dynamic MRI, images were sequentially obtained at unenhanced baselines and at 25, 60, and 180 s after bolus injection of 0.1 mmol/kg of gadodiamide hydrate (Omniscan, Daiichi Sankyo, Tokyo, Japan).

Image Interpretation and Data Analysis

MR images were interpreted and analyzed by the consensus of two experienced radiologists (C.T., with 4 years of experience in prostate MR imaging; and H.S., with 10 years of experience in prostate MR imaging) who were blinded to the patients' clinical history and PSA levels. The imaging diagnostic criteria for prostate cancer, BPH and noncancerous PZ were as follows. Prostate cancer was diagnosed when a mass lesion showed homogeneous hypointensity with indistinct margins on T2WI (10,21) and early enhancement on the arterial phase (25 s after bolus injection) of gadolinium-enhanced dynamic imaging in the region where the step-section pathology maps revealed the existence of cancerous tissues. Noncancerous PZ was diagnosed when PZ showed hyperintensity on T2WI and the step-section pathology did not reveal cancerous tissue in the corresponding PZ area. The diagnostic criteria of BPH nodules were a round mass with a distinct T2-hypointense capsule (termed "organized chaos") (11) and step-section maps revealing the BPH nodules without cancerous tissue in the corresponding lesion. BPH nodules tend to show heterogeneous signal intensity on T2WI because of their stromal and

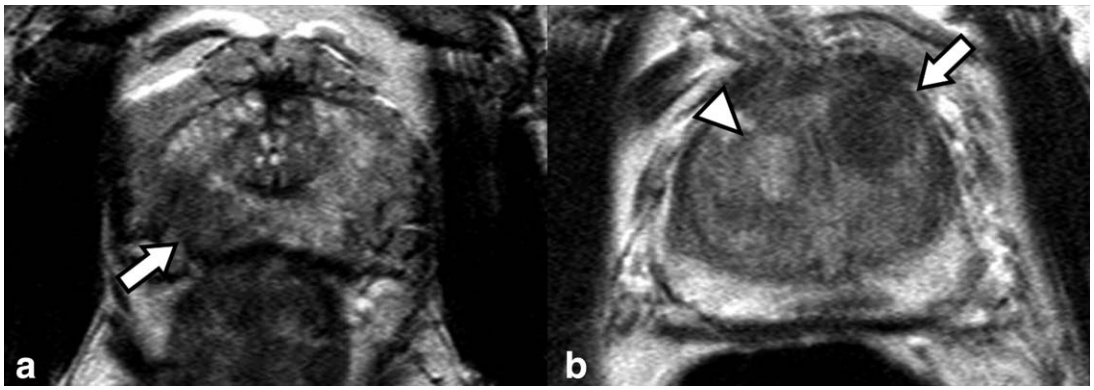

Figure 1. Typical cases of prostate cancer (arrow in **a**), stromal benign prostatic hyperplasia (BPH) (arrow in **b**), and nonstromal BPH (arrowhead in **b**) on T2-weighted images. Prostate cancer shows ill-defined hypointense lesion on T2WI, while stromal BPH and nonstromal BPH show well-defined hypointensity and hyperintensity on T2WI, respectively.

glandular components. Therefore, in our study, BPH nodules were classified into two subtypes with visual inspection, i.e., stromal BPH and nonstromal BPH, which show predominantly hypointensity and hyperintensity on T2WI, respectively (Fig. 1) (22).

We selected multiple lesions from the same patients if the lesions showed distinctly different origins. Four patients had two foci of prostate cancer. In BPH, two patients had one nodule, six patients had two nodules, one patient had three nodules, four patients had four nodules, and one patient had eight nodules. Finally, 24 foci of prostate cancer, 41 BPH nodules (14 stromal BPH nodules and 27 nonstromal BPH nodules), and 20 benign contralateral PZ were included in our study.

Regions of interest (ROIs) were drawn manually within proven prostate cancer, BPH, and PZ on DWI, using the MRI and histologic findings as references. The ROIs were subsequently transferred to DKI parametric map and ADC map to calculate the DKI parameters of *D*, *K*, and ADC. The ROIs were chosen to be as large as possible, consistent with minimal contamination from unintended tissues.

The acquired datasets were then transferred to a personal computer, and the data analysis was performed with PRIDE software (Phillips Medical Systems, Best, The Netherlands), which fits signal intensities (*S*) as a function of the b-value using the following DKI equation:

$$S = S_0 \cdot \exp\left(-b \cdot D + b^2 \cdot D^2 \cdot K/6\right),$$

where *K* represents deviations from normal distribution, and *D* represents non-Gaussian diffusion coefficient. The standard ADC was also calculated by using a conventional monoexponential fit with the equation:

$$S = S_0 \cdot \exp\left(-b \cdot ADC\right)$$

In addition, the signal-to-noise ratios (SNRs) of the prostate cancers, BPH, and benign PZ were calculated on DWIs with b-values of 1500 s/mm^2. Because the small FOV was filled with tissue signals, we used the mean of the standard deviation (SD) of the signals in the internal obturator muscles in place of the background signal (23), as follows:

$$\text{SNR} = (\text{signal intensity of region})/(\text{mean SD of bilateral internal obturator muscles})$$

The circular ROIs placed within the internal obturator muscles were larger than 50 mm^2.

The parameters *D*, *K*, and ADC were compared using a mixed model analysis of variance (ANOVA) with patients as a random effect. Post hoc Tukey honestly significant difference (HSD) test for pairwise comparisons were used to determine whether there was any significant difference between prostate cancer, BPH, and benign PZ (SAS, version 9.3; SAS Institute, Cary, NC). In addition, receiver operating characteristic (ROC) analyses were performed to evaluate the diagnostic performance of the parameters to discriminate prostate cancer from benign PZ (MedCalc, version 11.6.2.0, MedCalc Software, Mariakerke, Belgium). *P* values of < 0.05 were considered to indicate a significant difference.

RESULTS

DKI datasets were successfully acquired from 20 patients and the parametric maps for the kurtosis metrics were generated in all patients. The mean SNR for prostate cancers, BPH, and benign PZ with b = 1500 were 45.5 ± 14.9, 29.6 ± 7.6, and 27.3 ± 10.1 respectively. Figure 2 shows the DKI parametric map for a typical patient. Compared with healthy tissue, cancerous tissues showed higher *K* and lower *D* values. Figure 3 shows the distributions of *D*, *K*, and ADC in cancerous and noncancerous tissues, and Table 2 shows a summary of the results for *D*, *K*, and ADC. *D* was significantly lower in prostate cancer and stromal BPH than in benign PZ ($P < 0.001$ and $P = 0.035$, respectively). No significant difference in *D* was observed between nonstromal BPH and benign PZ ($P = 0.807$). Whereas, *K* was significantly higher in prostate cancer and stromal BPH than in benign PZ ($P < 0.001$ and $P < 0.001$, respectively). No significant difference in *K* was found between nonstromal BPH and benign PZ ($P = 0.571$). ADC was significantly

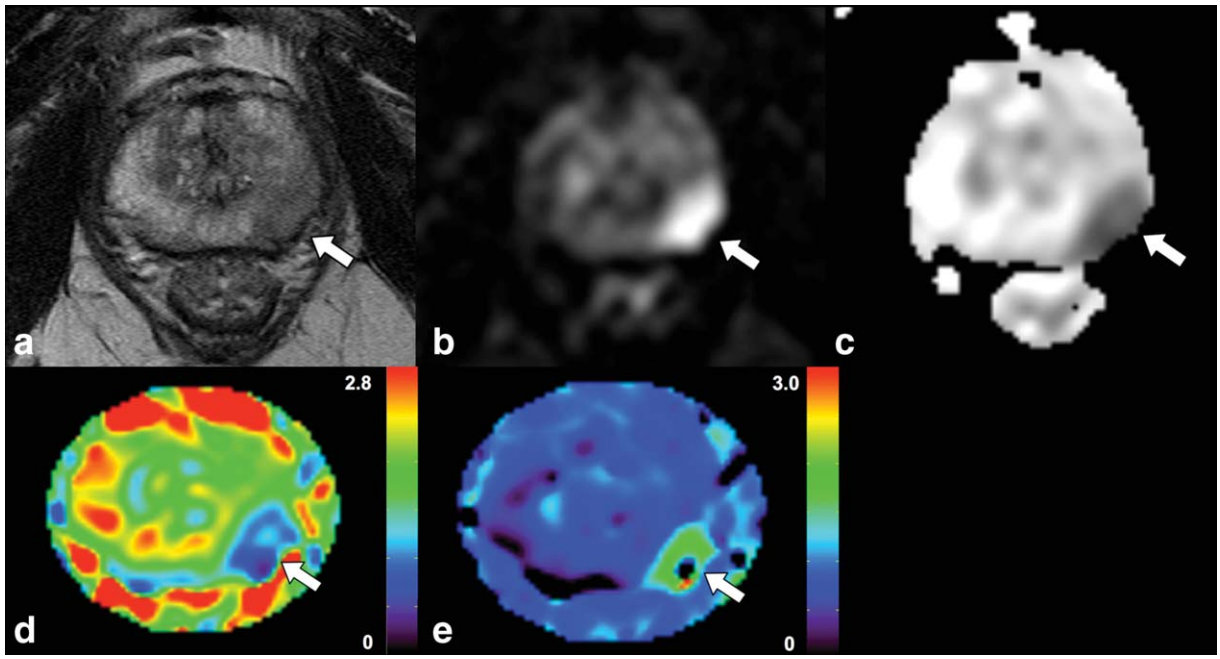

Figure 2. A 73-year-old man (prostate-specific antigen level, 12.1 ng/mL) with prostate cancer (arrows). T2-weighted image (T2WI) (**a**), diffusion-weighted image (DWI) (b = 1500 s/mm^2) (**b**), apparent diffusion coefficient (ADC) map (**c**), *D* map (**d**), and *K* map (**e**). Compared with healthy tissue, prostate cancer in left peripheral zone showed hypointensity on T2WI, hyperintensity on DWI, hypointensity on ADC, lower *D* value, and higher *K* value.

lower in prostate cancer and stromal BPH than in benign PZ ($P < 0.001$ and $P = 0.001$, respectively).

In the comparison of these parameters between prostate cancer and the both types of BPH, *D* was significantly lower and *K* was significantly higher in prostate cancer than in nonstromal BPH ($P < 0.001$ and $P < 0.001$, respectively). In addition, although not statistically significant, *K* showed a trend toward higher levels in prostate cancer than in stromal BPH ($P = 0.051$) (Fig. 4). ADC was significantly lower in prostate cancer than in nonstromal BPH ($P < 0.001$). No significant difference in ADC was found between prostate cancer and stromal BPH ($P = 0.070$).

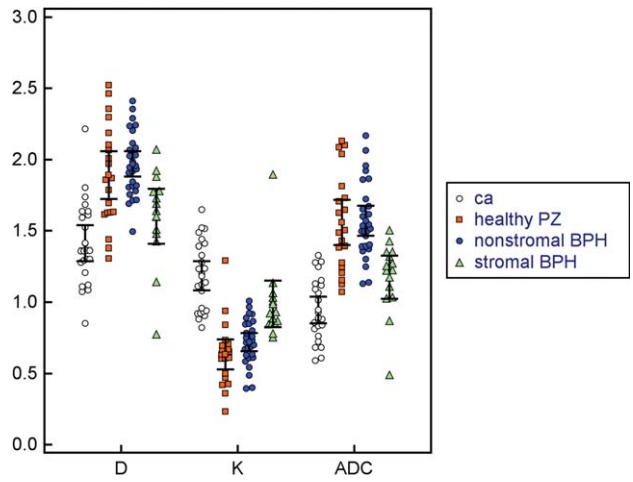

Figure 3. The distributions of *D*, *K*, and apparent diffusion coefficient (ADC) in cancerous and noncancerous tissues. Data points are *D* ($\times 10^{-3}$ mm^2/s), *K* (a unitless parameter), and ADC ($\times 10^{-3}$ mm^2/s). Error bars indicate 95% confidence intervals for mean.

Table 3 and Figure 5 demonstrate the results of the ROC analyses for discriminating prostate cancer from benign PZ. A significant difference in the area under the curve (AUC) was observed between *D* and ADC ($P = 0.023$) but not between *K* and *D* ($P = 0.125$) or between *K* and ADC ($P = 0.722$). However, *K* showed the greatest sensitivity among three parameters.

DISCUSSION

In recent years, DWI has emerged as a functional MRI technology for discriminating malignant from benign lesions (24,25). An increasing number of studies have shown that DWI has a high sensitivity and specificity for the diagnosis of prostate cancer (13–17). ADC values of prostate cancer are lower than those of benign tissue mainly because of dense cellularity of malignant lesions (26,27). In addition, ADC values are considered to correlate with Gleason scores (28).

DKI is an imaging analysis method of DWI for quantifying non-Gaussian water diffusion (18–20). DKI has been used in examinations of the brain and has shown promising results in cerebral ischemia, multiple sclerosis, and gliomas (29–31). In the present study, we successfully performed DKI analysis and found that *D* was significantly lower in prostate cancer than in benign PZ, and *K* was significantly higher in prostate cancer than in benign PZ. These results are consistent with a previous report by Rosenkrantz et al (32), though the standard of reference of their study was determined by the results of TRUS-guided biopsy. We have presented here the results of DKI metrics of the prostate gland with radical prostatectomy specimens as the standard of reference. In addition, we have shown that *D* and *K* were significantly

Table 2
Results for the DKI Parameters of *D*, *K*, and ADC*

Parameter	Prostate cancer	Benign PZ	Stromal BPH	Non-stromal BPH
D ($\times 10^{-3}$ mm^2/s)	1.41 ± 0.29†	1.89 ± 0.36‡	1.60 ± 0.33†	1.97 ± 0.22‡
K	1.19 ± 0.24†	0.63 ± 0.23‡	0.99 ± 0.28†	0.72 ± 0.16‡
ADC ($\times 10^{-3}$ mm^2/s)	0.95 ± 0.23†	1.56 ± 0.34‡	1.18 ± 0.26†	1.57 ± 0.27‡

*Data are the means ± standard deviation.
†Significantly different in comparison with benign PZ at *P* less than 0.05.
‡Significantly different in comparison with prostate cancer at *P* less than 0.05.

different between stromal BPH and benign PZ. Comparing these parameters between prostate cancer and both types of BPH, significant differences in *D* and *K* were observed between prostate cancer and nonstromal BPH. In addition, although not statistically significant, *K* showed a trend toward higher levels in prostate cancer than in stromal BPH ($P = 0.051$). These findings might be of clinically importance because discriminating BPH from prostate cancer in TZ is more challenging with MRI. DKI may provide additional information for differentiating prostate cancer from BPH.

The results of the ROC analyses for discriminating prostate cancer from benign PZ showed that there was no significant difference in the AUC between *K* and *D* or between *K* and ADC. However, *K* showed the highest sensitivity among three parameters. Because an advantage of using DWI is its relative high sensitivity for detecting prostate cancer (13–17), DKI might be suitable for this purpose. Especially, in the case of negative result of TRUS-guided biopsy with an interval rise in PSA, DKI might be useful tool for detecting prostate cancer. Further studies with a larger series of patients are needed to confirm these findings.

There are also other mathematical models for describing nonmonoexponential diffusion attenuated MR signals. These include a biexponential model (33), a statistical model (34,35), and a stretched exponential model (36). These models have been mainly applied to brain DWI studies (35,37,38). Recently, the biexponential model, including intravoxel incoherent motion (IVIM) model, has been applied to the DWI studies of the prostate gland (39–41). IVIM model, as originally described by Le Bihan et al, is considered a form of biexponential model (42). IVIM model uses low b-values to sensitize microcirculation of blood within the capillaries (perfusion), and pure molecular diffusion and perfusion can be separately evaluated. Particular attention needs to be paid not to confuse IVIM model with a biexponential model using diffusion measurements over an extended b-value range up to 3000 s/mm^2 (39,40). Although these biexponential models provide a statistically better fit over the monoexponential model in relationships between diffusion signal decays and b-values, there are some controversial points in biexponential model (43). Oshio suggested that the parameters estimation by biexponential curve fitting is not reliable because of the existence of multiple local minima near the global minimum (44). In other words, multiple parameter sets can generate similar biexponential curves. Another problem is the biologic interpretation of the parameters of fast and slow ADCs. Although the physiologic basis of fast (perfusion) and slow (pure molecular diffusion) components of IVIM is rather clear, the physiologic basis of fast and slow ADCs using high

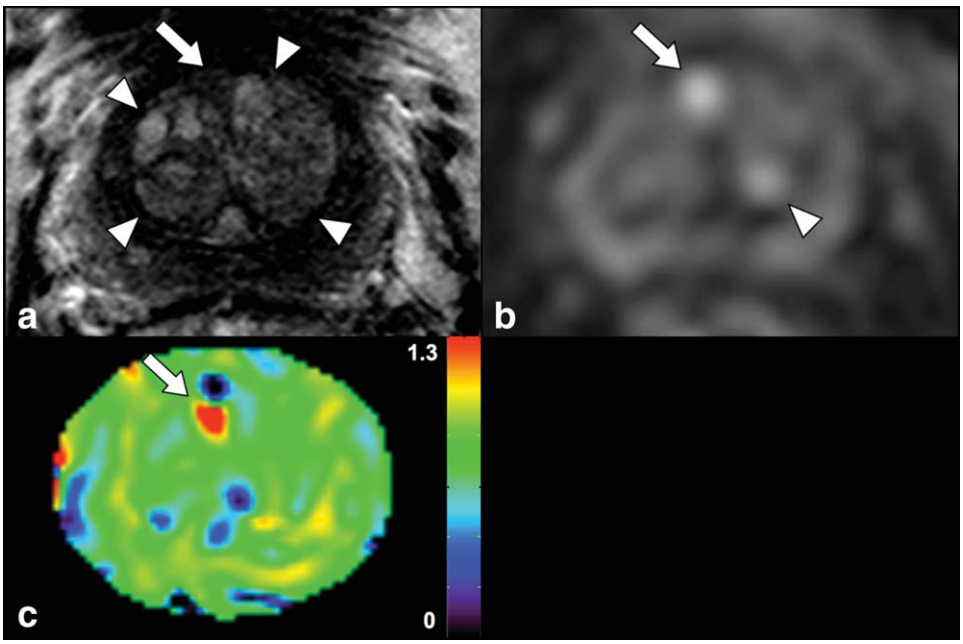

Figure 4. A 70-year-old man (prostate-specific antigen level, 6.0 ng/mL) with prostate cancer (arrows). T2-weighted image (T2WI) (**a**), diffusion-weighted image (DWI) (b = 1500 s/mm^2) (**b**), *K* map (**c**). Compared with healthy tissue, prostate cancer in transitional zone showed hypointensity on T2WI, hyperintensity on DWI, and higher *K* value. However, although there were two kinds of benign prostatic hyperplasia in transitional zone (arrowheads in **a**) and one of them showed hyperintensity on DWI (arrowhead in **b**), only prostate cancer showed higher *K* value compared with healthy tissue (arrow in **c**).

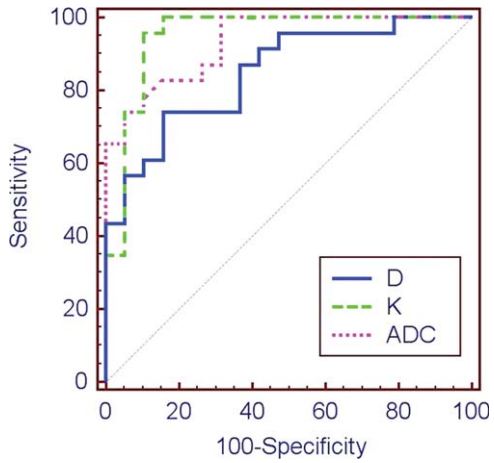

Figure 5. Comparison of receiver operating characteristic curves for discriminating prostate cancer from benign PZ. The area under the curve (AUC) was 0.856 for *D*, 0.952 for *K*, and 0.939 for apparent diffusion coefficient (ADC). A significant difference in the AUC was observed between *D* and ADC ($P = 0.023$) but not between *K* and *D* ($P = 0.125$) or between *K* and ADC ($P = 0.722$).

b-value range is still unclear. However, this problem is also true for the DKI. DKI metric, *K*, is thought to be an index of microstructural complexity, however, the physiologic basis of *K* is also uncertain. Further improvements in mathematic modeling of DWI signal decay are desired for a better understanding of the physiologic basis of DWI.

Our study has several limitations. First, only 20 patients who underwent radical prostatectomy were included in this study. Larger patient populations with a broad range of tumor grades are needed to establish the usefulness of DKI for the diagnosis of prostate cancer. Second, we used 11 b-values with a maximal b-value of 1500 s/mm^2. Rosenkrantz et al. used a maximal b-value of 2000 s/mm^2 in their DKI study of the prostate gland (32). However, the appropriate number and the upper bound of b-values for the prostate gland are still unknown. Eleven b-values used in this study may be too large in number, but it is not detrimental to sample as dense as clinically feasible to investigate diffusion signal decay modeling. Third, 15 of 20 patients had a Gleason score of 7 in this study. Thus, the correlation between the Gleason score and *D* or *K* values could not be evaluated. Fourth, the BPH nodules were classified as stromal BPH or nonstromal BPH according to the signal intensity on T2WI. However, the visual inspection of the signal intensity may introduce a selection bias in the measurements and may have influenced our results.

In conclusion, we have shown the differences in parameters between prostate cancer, BPH, and benign PZ using DKI. *K* was significantly higher in prostate cancer than in nonstromal BPH and healthy PZ and showed a trend toward higher levels in prostate cancer than in stromal BPH. DKI may contribute to the diagnosis of prostate cancer, especially in the differential diagnosis of prostate cancer and BPH.

Table 3
Results of the Receiver Operating Characteristic Analyses for Discriminating Prostate Cancer From Benign PZ*

	AUC	Threshold	Sensitivity (%)	Specificity (%)
D	0.856	≤1.610 ($\times 10^{-3}$ mm^2/sec)	75.0	85.0
K	0.952	>0.842	95.8	90.0
ADC	0.939	≤1.120 ($\times 10^{-3}$ mm^2/sec)	75.0	95.0

*The optimal threshold of each parameter was selected to maximize the average of sensitivity and specificity. *K* showed the greatest sensitivity for detecting prostate cancers among three parameters.
AUC = area under the curve.

REFERENCES

1. Jemal A, Center MM, Desantis C, Ward EM. Global patterns of cancer incidence and mortality rates and trends. Cancer Epidemiol Biomarkers Prev 2010;19:1893–1907.
2. Center MM, Jemal A, Lortet-Tieulent J, et al. International variation in prostate cancer incidence and mortality rates. Eur Urol 2012;61:1079–1092.
3. Brawley OW. Trends in prostate cancer in the United States. J Natl Cancer Inst Monogr 2012;45:152–156.
4. Heidenreich A, Bellmunt J, Bolla M, et al. EAU guidelines on prostate cancer. Part 1: screening, diagnosis, and treatment of clinically localized disease. Eur Urol 2011;59:61–71.
5. Eskicorapci SY, Baydar DE, Akbal C, et al. An extended 10-core transrectal ultrasonography guided prostate biopsy protocol improves the detection of prostate cancer. Eur Urol 2004;45:444–448.
6. Passoni NM, Di Trapani E, Suardi N, et al. Clinical and diagnostic assessment for therapeutic decisions in prostate cancer. Q J Nucl Med Mol Imaging 2012;56:321–330.
7. McSherry SA, Levy F, Schiebler ML, Keefe B, Dent GA, Mohler JL. Preoperative prediction of pathological tumor volume and stage in clinically localized prostate cancer: comparison of digital rectal examination, transrectal ultrasonography and magnetic resonance imaging. J Urol 1991;146:85–89.
8. Schnall MD, Pollack HM. Magnetic resonance imaging of the prostate gland. Urol Radiol 1990;12:109–114.
9. Jager GJ, Ruijter ET, van de Kaa CA, et al. Dynamic TurboFLASH subtraction technique for contrast-enhanced MR imaging of the prostate: correlation with histopathologic results. Radiology 1997; 203:645–652.
10. Akin O, Sala E, Moskowitz CS, et al. Transition zone prostate cancers: features, detection, localization, and staging at endorectal MR imaging. Radiology 2006;239:784–792.
11. Barentsz JO, Richenberg J, Clements R, et al. ESUR prostate MR guidelines 2012. Eur Radiol 2012;22:746–757.
12. Oto A, Kayhan A, Jiang Y, et al. Prostate cancer: differentiation of central gland cancer from benign prostatic hyperplasia by using diffusion-weighted and dynamic contrast-enhanced MR imaging. Radiology 2010;257:715–723.
13. Sato C, Naganawa S, Nakamura T, et al. Differentiation of noncancerous tissue and cancer lesions by apparent diffusion coefficient values in transition and peripheral zones of the prostate. J Magn Reson Imaging 2005;21:258–262.
14. Tanimoto A, Nakashima J, Kohno H, Shinmoto H, Kuribayashi S. Prostate cancer screening: the clinical value of diffusion-weighted imaging and dynamic MR imaging in combination with T2-weighted imaging. J Magn Reson Imaging 2007;25:146–152.
15. Reinsberg SA, Payne GS, Riches SF, et al. Combined use of diffusion-weighted MRI and 1H MR spectroscopy to increase accuracy in prostate cancer detection. AJR Am J Roentgenol 2007;188:91–98.
16. Yoshimitsu K, Kiyoshima K, Irie H, et al. Usefulness of apparent diffusion coefficient map in diagnosing prostate carcinoma: correlation with stepwise histopathology. J Magn Reson Imaging 2008; 27:132–139.
17. Tan CH, Wei W, Johnson V, Kundra V. Diffusion-weighted MRI in the detection of prostate cancer: meta-analysis. AJR Am J Roentgenol 2012;199:822–829.

18. Jensen JH, Helpern JA, Ramani A, Lu H, Kaczynski K. Diffusion kurtosis imaging: the quantification of non-gaussian water diffusion by means of magnetic resonance imaging. Magn Reson Med 2005;53:1432–1440.
19. Lu H, Jensen JH, Ramani A, Helpern JA. Three-dimensional characterization of non-gaussian water diffusion in human using diffusion kurtosis imaging. NMR Biomed 2006;19:236–247.
20. Jensen JH, Helpern JA. MRI quantification of non-Gaussian water diffusion by kurtosis analysis. NMR Biomed 2010;23:698–710.
21. Li H, Sugimura K, Kaji Y, et al. Conventional MRI capabilities in the diagnosis of prostate cancer in the transition zone. AJR Am J Roentgenol 2006;186:729–742.
22. Ishida J, Sugimura K, Okizuka H, et al. Benign prostatic hyperplasia: value of MR imaging for determining histologic type. Radiology 1994;190:329–331.
23. Kaji Y, Kuroda K, Maeda T, et al. Anatomical and metabolic assessment of prostate using a 3-Tesla MR scanner with a custom-made external transceive coil: healthy volunteer study. J Magn Reson Imaging 2007;25:517–526.
24. Takahara T, Imai Y, Yamashita T, et al. Diffusion weighted whole body imaging with background body signal suppression (DWIBS): technical improvement using free breathing, STIR and high resolution 3D display. Radiat Med 2004;22:275–282.
25. Guo Y, Cai YQ, Cai ZL, et al. Differentiation of clinically benign and malignant breast lesions using diffusion-weighted imaging. J Magn Reson Imaging 2002;16:172–178.
26. Guo Y, Cai YQ, Cai ZL, et al. Differentiation of clinically benign and malignant breast lesions using diffusion-weighted imaging. J Magn Reson Imaging 2002;16:172–178.
27. Koh DM, Collins DJ. Diffusion-weighted MRI in the body: applications and challenges in oncology. AJR Am J Roentgenol 2007; 188:1622–1635.
28. Tamada T, Sone T, Jo Y, et al. Apparent diffusion coefficient values in peripheral and transition zones of the prostate: comparison between normal and malignant prostatic tissues and correlation with histologic grade. J Magn Reson Imaging 2008;28: 720–726.
29. Jensen JH, Falangola MF, Hu C, et al. Preliminary observations of increased diffusional kurtosis in human brain following recent cerebral infarction. NMR Biomed 2011;24:452–457.
30. Helpern JA, Adisetiyo V, Falangola MF, et al. Preliminary evidence of altered gray and white matter microstructural development in the frontal lobe of adolescents with attention-deficit hyperactivity disorder: a diffusional kurtosis imaging study. J Magn Reson Imaging 2011;33:17–23.
31. Raab P, Hattingen E, Franz K, Zanella FE, Lanfermann H. Cerebral gliomas: diffusional kurtosis imaging analysis of microstructural differences. Radiology 2010;254:876–881.
32. Rosenkrantz AB, Sigmund EE, Johnson G, et al. Prostate cancer: feasibility and preliminary experience of a diffusional kurtosis model for detection and assessment of aggressiveness of peripheral zone cancer. Radiology 2012;264:126–135.
33. Niendorf T, Dijkhuizen RM, Norris DG, van Lookeren Campagne M, Nicolay K. Biexponential diffusion attenuation in various states of brain tissue: implications for diffusion-weighted imaging. Magn Reson Med 1996;36:847–857.
34. Yablonskiy DA, Bretthorst GL, Ackerman JJ. Statistical model for diffusion attenuated MR signal. Magn Reson Med 2003;50:664–669.
35. Yablonskiy DA, Sukstanskii AL. Theoretical models of the diffusion weighted MR signal. NMR Biomed 2010;23:661–681.
36. Bennett KM, Schmainda KM, Bennett RT, Rowe DB, Lu H, Hyde JS. Characterization of continuously distributed cortical water diffusion rates with a stretched-exponential model. Magn Reson Med 2003;50:727–734.
37. Mulkern RV, Gudbjartsson H, Westin CF, et al. Multi-component apparent diffusion coefficients in human brain. NMR Biomed 1999;12:51–62.
38. Kwee TC, Galban CJ, Tsien C, et al. Intravoxel water diffusion heterogeneity imaging of human high-grade gliomas. NMR Biomed 2010;23:179–187.
39. Mulkern RV, Barnes AS, Haker SJ, et al. Biexponential characterization of prostate tissue water diffusion decay curves over an extended b-factor range. Magn Reson Imaging 2006;24:563–568.
40. Shinmoto H, Oshio K, Tanimoto A, et al. Biexponential apparent diffusion coefficients in prostate cancer. Magn Reson Imaging 2009;27:355–359.
41. Shinmoto H, Tamura C, Soga S, et al. An intravoxel incoherent motion diffusion-weighted imaging study of prostate cancer. AJR Am J Roentgenol 2012;199:W496–W500.
42. Le Bihan D, Breton E, Lallemand D, Aubin ML, Vignaud J, Laval-Jeantet M. Separation of diffusion and perfusion in intravoxel incoherent motion MR imaging. Radiology 1988;168:497–505.
43. Acton FS. Numerical methods that works, 2nd ed. Washington, DC: The Mathematical Association of America; 1990. p 253.
44. Oshio K.Reliability of bi-exponential parameter estimation. In: Proceedings of the 20th Annual Meeting of ISMRM, Melbourne, 2012. p 3583.